Published in final edited form as:
J Orthop Res. 2012 February ; 30(2): 325–333. doi:10.1002/jor.21500.

The unique angiogenic and vasculogenic properties of renal cell carcinoma in a xenograft model of bone metastasis are associated with high levels of *vegf-a* and decreased *ang-1* expression

Chao Xie[1,2], **Edward M. Schwarz**[1,2], **Robinder S. Dhillon**[1], **Erik R. Sampson**[1,2], **Dan Li**[1,2], **Regis J. O'Keefe**[1,2], and **Wakenda Tyler**[1,2,3]

[1]Center for Musculoskeletal Research, University of Rochester School of Medicine and Dentistry, Rochester, NY

[2]Department of Orthopaedics, University of Rochester School of Medicine and Dentistry, Rochester, NY

Abstract

Management of various tumor metastases to bone has dramatically improved, but this is not so for renal cell carcinoma (RCC), which is a difficult surgical problem due to its great vascularity. Furthermore, the unique mechanisms that mediate RCC vasculogenesis in bone remain unknown. To understand this process we developed a xenograft model that recapitulates highly vascular RCC vs. less vascular tumors that metastasize to bone. Human tumor cell lines of RCC (786-O), prostate cancer (PC3), lung cancer (A549), breast cancer (MDA-MB231) and melanoma (A375) were transfected with firefly luciferase (Luc), injected into the tibiae of nude mice, and differences in growth, osteolysis and vascularity were assessed by longitudinal bioluminescent imaging (BLI), micro-CT for measurement of calcified tissues and vascularity and histology. The results showed that while RCC-Luc has reduced growth and osteolytic potential vs. the other tumor lines, it displayed a significant increase in vascular volume ($p<0.05$). This expansion was due to 3- and 5-fold increases in small and large vessel numbers respectively. *In vitro* gene expression profiling revealed that RCC-Luc expresses significantly ($p<0.05$) more *vegf-a* (10-fold) and 20-30-fold less *ang-1* vs. the other lines. These data demonstrate the utility of this model to study the unique vasculogenic properties of RCC bone metastases.

Keywords

Renal Cell Carcinoma (RCC); vasculogenesis; bone metastasis; xenograft

Introduction

There are an estimated 49,000 new cases of renal cell carcinoma (RCC) diagnosed in the United States each year and 11,000 deaths were reported in 2009 [1]. Although major advances in the treatment of metastatic RCC have occurred over the past decade with the introduction of several receptor tyrosine kinase inhibitors [2], the disease remains a fatal condition and is wrought with morbidities that are often very challenging to treat. Five year

[3]To whom correspondence should be addressed: Dr. Wakenda Tyler, Department of Orthopaedics, University of Rochester Medical Center, 601 Elmwood Avenue, Box 665, Rochester, NY 14642, Phone 585-275-3100, FAX 585-756-4727, Wakenda_Tyler@URMC.Rochester.edu.

survival of patients with metastatic RCC is less than 10% [3]. Bone is the second most common site, next to lung of metastatic disease for RCC [4]. RCC carcinoma is the 4th most common malignancy to spread to bone following lung, breast and prostate. Despite recent advances, RCC is still notorious for having a poor response to radiation therapy as well as other adjuvant chemotherapeutic regimens. In most instances of bone metastasis from RCC, the only options available are surgical resection and boney reconstruction. The surgical resection itself can be plagued with complications, often due to the vascular nature of these tumors.

Systemic treatment for RCC has historically been based on cytokine therapy, specifically high dose interlukin-2 (IL-2) and interferon-α. These modalities have provided modest benefits in survival for patients with metastatic RCC. A major breakthrough in our understanding of the highly vascular nature of RCC came with the discovery that loss of function of the von Hippel-Lindau (*VHL*) gene is an early event during tumorgenesis. Inheritance of a defective copy of the *VHL* gene is the most common cause for inherited RCC [5]. Furthermore, up to 75% of patients with sporadic RCC have aberrant *VHL* (e.g., chromosome 3p deletion, suppressed expression, or loss-of-function base substitutions) [6]. Thus, loss of VHL function is an important sentinel event during RCC pathogenesis. Loss of this gene results in constitutive activation of hypoxia inducible factor (HIF 1-α), a transcription factor which induces the target genes vascular endothelial growth factor (VEGF) and platelet derived growth factor (PDGF), as well as several other genes. VEGF has specifically been associated with neovascularization of small diameter vessels. Much of RCC vascularity has been attributed to VHL tumor suppressor gene inactivation and resultant VEGF over-expression [6, 7]. However, lacking from this assessment is the observation that RCC has both small and large vessels present within the tumor. Additionally, the process by which small vessels are remodeled into large smooth muscle and pericyte lined blood vessels, known as vasculogenesis, in RCC is poorly understood. It is hypothesized that the vaculogenesis pathway plays a critical role in the pathogenesis of this tumor. Thus, establishing a translational animal model that faithfully displays the unique vasculogenic properties of RCC metastases in bone could be the key towards identifying novel targets for therapy.

To this end, we modified the established athymic nude mouse xenograft model to evaluate growth, osteolytic, angiogenic and vasculogenic differences between prototypic human cancer cell lines that metastasize to bone, namely prostate cancer (PC3) [8], lung cancer (A549) [9], breast cancer (MDA-MB231) [10] and melanoma (A375) [11]. By comparing the growth, angiogenic, vasculogenic and osteolytic phenotypes of these tumor lines in bone, here we establish for the first time that this model faithfully distinguishes the unique vasculogenic properties of RCC bone metastases.

Methods

Stably transduced cell lines

Human tumor cell lines for lung (A549) and melanoma (A375) were obtained from the American Type Culture Collection (ATCC). PC3 cells were obtained from Dr. J. Lieberman [12]. 786-O cells were obtained from Dr. G. Wu [13]. MDA-MB231 cells were obtained from Dr. L. Xing [14]. All cell lines were initially cultured in MEM-alpha solution with 10% bovine serum at 37°C, 4% CO_2. To generate lentivirus encoding *Firefly* luciferase, 293FT producer cells were transfected with pLenti6/V-5Dest-LUC plasmid and ViraPower™ packaging mix (Invitrogen K4975-00) using Lipofectamine 2000™ (Invitrogen 11668-027). The next morning, the 293FT media was changed and two days thereafter, viral supernatant was collected, 0.45μm-filtered, supplemented with 8μg/mL Polybrene (hexadimethrine bromide, Sigma H9268) and applied to target cells. Transduced

target cells were selected using blasticidine (Invitrogen A11139-02) and drug resistant clones were screened via *in vitro*, luciferase assays as previously described [15], and the data from the highest expressing clones from each cell line are presented in Figure 1A. The transdused five cell lines then were defined as LC-Luc (A549), MC-Luc (A375), PC-Luc (PC-3), RCC-Luc (786-O) and BC-Luc (MDA-MB231) in the following study.

Quantitative PCR

Cells were cultured and collected as described above for the five cell lines. At confluence (approximately 1×10^7 cells), plates were scrapped and RNA collected using RNeasy mini purification kit (Qiagen, Valencia, Ca) according to manufacturer's protocol. Single-strand cDNA was synthesized from 1.0 μg of mRNA using an iScript cDNA synthesis kit (Bio-Rad Lab, Hercules, CA). Primers were obtained from Integrated DNA Technologies (IDT, Copyright 2011).

Real time PCR was performed to quantify the expression of *angiopoietin-1* (*ang1*), *ang2*, *vegf-a,b,c,d*, *vegfr1,2,3* and *tie2* in all cell lines. Each reaction was carried out in a final volume of 20 μl consisting of 0.1 μM primers, 1× Sybr Green PCR Super Mix (ABgene, Thermo Fisher Scientific Inc, Rochester, NY) and 1μl of the purified cDNA template. The samples were assayed in triplicate in a Rotor-Gene RG 3000 (Corbett Research, Sydney, AU). Messenger RNA levels were compared relative to a control gene, GAPDH for standardization of samples.

Xenografting and Bioluminescent Imaging (BLI)

Six week old, athymic nude mice were obtained from the National Cancer Institute and housed in the animal Vivarium one week prior to the start of experimentation. A total of 10 mice per group were used for the in-vivo experiments. With a 50% engraftment rate, this allowed for 5 mice with viable tumors at time of sacrifice on day 35. Experiments were repeated twice for the RCC-lLuc and PC-Luc cell lines to verify findings. Approval for all animal experiments was obtained from the Institutional Animal Care and Utilization Committee (IACUC) prior to conducting experiments. Mice were anesthetized using ketamine hydrochloride (100mg/kg) and xylazine (10mg/kg) via peritoneal injection. The right hind limb skin was cleaned with 70% ethanol. A 3~4mm vertical incision was made to expose the patellar tendon. Then a 3-mm longitudinal cut was made with a Bard-Parker® no.15 scalpel blade over the side of patellar ligament. The patellar tendon was retracted to the side of knee joint to expose the tibial plateau. A 26-gauge needle was inserted 2–3 mm into the proximal end of the tibia using a drilling motion and total 1×10^5 cells in 10μL 1× PBS was injected into tibial bone marrow cavity by using a 10μl Hamilton® syringe. This same procedure was performed in mice for all cell lines. An Ethicon 4-0 silk suture was used to close the incision at the end of the procedure. Mice were monitored post-operatively for appropriate behavior and given pain medications when indicated.

On days 1, 7, 14, 28 and 35 after tumor injection, bioluminescence imaging (BLI) is performed using the Xenogen IVIS camera system (Xenogen Corporation, Alameda, Calif.). Thirty second high sensitivity dorsal images were taken at each time point. The BLI was quantified with the LivingImage software 2.50.1 (Xerogen Corporation, Alameda, Calif.) by analyzing a fixed region of interest (ROI) centered as a 5mm diameter on the tumor at the proximal end of tibia. The BLI photon signal was then calculated as average radiance (p/sec/cm2/sr). On day 14, mice that did not show continued growth of photon signal by BLI imaging with a signal by day 14 of at least 1000 p/sec/cm2/sr were considered non-engrafters and were removed from the study. Mice that showed greater than 1000 p/sec/cm2/sr on day 14 were continuously monitored until day 35 post tumor injection.

Tissue Harvesting

On day 35, all mice were anesthetized with ketamine hydrochloride (100mg/kg) and xylazine (10mg/kg) via peritoneal injection. Final BLI imaging was performed followed by plain radiographic using the Faxitron Cabinet X-ray System to determine the amount of osteolysis. Animals were then euthanized using lead chromate intra-cardiac infusion as previously described [16]. This technique was performed by performing a thoracotomy on anesthetized animals. The left ventricle was indentified and a small 20 gauge angiocatheter was inserted into the left ventricular chamber. The circulatory system was flushed with 20 ml of 0.9% saline and heparin (100IU/ml), followed by 20 ml of 10% neutral formalin. This procedure was immediately followed by injection of 4ml lead base contrast agent microfilm MV-122 (Flow Tech, Inc., Carver, Massachusetts) via the same route to perfuse the mouse's whole circulatory system. The operation was stopped when the mouse's liver and both feet completely fill with contrast agent. Mice were placed in 10% neutral formalin and stored until micro-CT analysis was conducted.

Micro-CT

The tumor containing hind limbs were disarticulated from the body of the mouse and all non-tumor soft tissue (muscle and ligaments) were removed from the specimens for vascular micro-CT analysis as previously described [16]. Specimens were then subjected to micro-CT analysis using a 10.5 micro high resolution μCT (VivaCT 40; Scanco Medical AG, Basserdorf, Switzerland). Following initial micro-CT analysis, the specimens were then decalcified for 4–6 weeks in ethylenediaminetetraacetic acid (EDTA). Following decalcification, specimens were again subjected to micro-CT analysis. After the completion of micro-CT analysis, specimens are then processed for histologic analysis.

Histologic Analysis

Following micro-CT, the tumor containing tibias were dissected and embedded in paraffin. A mid-sagittal and mid-coronal cut was made through the tumor specimen. At the mid-point of the tumor on both the sagittal and coronal cuts, four 4-micron tissue slices were obtained and mounted on slides. One slide for each orientation of cut was processed for hematoxylin and eosin (H&E) staining as previously described [16].

Statistical Analysis

All statistical analysis was performed using Prism statistical package Version 4.0 (GraphPad, San Diego, CA) with p-values of less than 0.05 being considered statistically significant. A one way analysis of variance (ANOVA) and Newman-Keuls Multiple Comparison Test was used for all statistical analyses. Statistical significance is indicated in the figures and figure legends.

Results

In vivo growth behavior of tumor lines in bone

To assess the relative differences in engraftment and *in vivo* luciferase expression of the five tumor cell lines in our xenograft model, we performed longitudinal BLI after intra-tibial injection (Fig. 1B). Engraftment rates were approximately 50% for all five tumor cell lines as determined by a BLI >1000 photons/s/cm^2/sr on day 14. Of note is that attempts to utilize TT cells (obtained from ATCC, Ref No: CRL-1803), a human thyroid cancer cell line, consistently resulted in failed engraftment, and were eliminated from this study (data not shown). Analyses of the BLI signal on days 14 and 35 demonstrated that the luciferase activity of PC-Luc was significantly greater than RCC-Luc (Fig. 1C).

Modest osteolytic properties of RCC-Luc xenografts

Since osteolytic potential is a biomarker of aggressive tumor metastasis to bone, we performed micro-CT to assess the amount of bone loss caused by each tumor on day 35 after intra-tibial injection. Representative 3D reconstructed images of the engrafted tibiae illustrate the relative osteolytic potential of each cell line (Fig. 2A), and these phenotypes were confirmed by quantifying the residual bone volumes (Fig. 2B). The results showed that BC-Luc tumors induced the most osteolysis, followed by MC-Luc tumors. In contrasts, RCC-Luc, PC-Luc and LC-Luc all showed modest degrees of osteolysis. One unexpected finding was the lack of bone loss observed in the LC-Luc xenografts, which was not significantly different from the vehicle control, despite clear evidence of osteolytic lesions. However, there was also evidence of bone formation at the tumor margins, suggesting that A549 is a mixed osteolytic-osteoblastic tumor cell line. Also of note was that bone volume loss did not correlate with the BLI signal intensity, suggesting that growth and osteolytic potential are independent variables in this model.

Large vessel vasculogenesis is a unique property of RCC-Luc xenografts

In order to assess the vascularity of the xenografts, we quantified the microfil in the demineralized tibiae by micro-CT. Representative 3D reconstructed images from each group demonstrate the remarkable angiogenic and vasculogenic potential of the RCC-Luc cell line, which was not observed with any of the other tumor lines (Fig. 3A). Quantitative analyses confirmed the significant 3-fold increases in total vessel volume vs. the vehicle control (Fig. 3B). In order to distinguish small vessel angiogenesis from large vessel vasculogenesis, we quantified the number of these distinct blood vessels separately. This analysis demonstrated that RCC-Luc tumors have a significant 3-fold increase in small vessels (Fig. 3C) and a 5-fold increase in large vessels vs. the vehicle control (Fig 3D). In contrast, none of the other tumor cells displayed significant angiogenic or vasculogenic potential above the vehicle control. Despite its greater BLI and osteolytic potential, the vascularity of PC-Luc xenografts was not significantly different than that of the vehicle control. Additionally, the BC-Luc, LC-Luc and MC-Luc tumors showed significantly lower vessel volumes, and fewer small and large vessels, compared to the vehicle control. Collectively, these results demonstrate the unique angiogenic and vasculogenic properties of RCC, which is another independent variable of tumor metastasis to bone.

Hematoxylin and eosin (H&E) staining performed on the harvested tumor specimens reveal the presence of blood vessels with lead-chromate present within the lumens of the vessels as a result of the microfil vascular perfusion process (Fig. 4). In order to better interpret the vascular micro-CT data, we compared the microfil containing vessels in the solid tumors (Figs. 4A2–F2) to this vasculature in the adjacent parenchymal bone tissue (Figs. 4A3–F3). It was noted on the H&E stains that LC-Luc showed an abundant amount of intracellular mucin production (light blue staining, Fig. 4E2), which is not atypical of an epithelial cancer cell with secretory function, such as lung cancer. Consistent with the micro-CT data, we observed a dramatic increase in the number of small and large vessels in RCC-Luc xenografts vs. the vehicle controls. However, the most remarkable finding was the complete absence of large vessels in the PC-Luc, BC-Luc, LC-Luc and MC-Luc tumor stroma (Figs. 4C2–F2), although these large vessels were present in the adjacent parenchymal tissue (Figs. 4C3–F3). These results confirm the unique angiogenic and vasculogenic properties of RCC compared to the other tumor types that metastasize to bone, which are remarkably avascular.

Angiogenic and vasculogenic gene expression profiles of the tumor lines

In order to gain insights on the possible mechanisms responsible for the unique angiogenic and vasculogenic properties of RCC versus the other tumors that metastasize to bone, we performed a limited transcriptome analysis of the cell lines in vitro to assess gene expression

levels of the vascular endothelial growth factors (VEGF), angiopoietins (Ang) and their receptors (Fig. 5). Consistent with prior reports [13, 17], we found that *vegf-a* mRNA levels were 10-fold higher in RCC-Luc cells vs. the other tumor lines. This high level of *vegf-a* corresponded with a commensurate autoregulatory down-regulation of its primary receptor *vegfr-2* in RCC-Luc cells compared to PC-Luc, BC-Luc and MC-Luc. Interestingly, we found that LC-Luc expresses very high levels of *vegf-d* and its receptor *vegfr-3*, which are primarily involved in lymphangiogenesis.

In terms of vasculogenesis, we found that *ang-1* is significantly down-regulated 20 to 30-fold in RCC-Luc vs. the other tumor cell lines. This observation is consistent with the prominent anti-angiogenic effects of Ang-1 in various tumor models [18–21], and its absence in RCC may be central to Ang-2 mediated vasculogenesis in these tumors.

Conclusion

Of the five major tumors that metastasize to bone RCC has one of the worst prognosis, as the mean survival rate is only 12 months [22]. This deadly nature of RCC is contrasted by the other tumors that metastasize to bone such as PC, which has a mean survival rate of 6.6 years [23]. This begs investigation into the different pathogenic mechanism of these tumors, of which the extraordinary vascularity of RCC is paramount [6, 7]. Unfortunately, progress in this field has been slow, in part due to the absence of an animal model that faithfully displays the remarkable vascular properties of RCC boney metastasis vs. the other tumors, such that deductive analyses can be performed to elucidate the novel factors responsible for the vascular/aggressive phenotype.

Angiogenesis has long been recognized as a target for anti-tumor therapy, which has resulted in several new drugs for RCC over the last decade [24]. Lose of function of the VHL gene plays a critical role in the development of the inherited form of RCC [5]. Since VHL is a component of an E3 ubiquitin-protein ligase complex that binds with and polyubiquinates the transcriptional factor hypoxia-inducible factor (HIF)-1α, HIF-2α, and HIF-3α, its loss results in a dramatic increase in VEGF-A expression [25, 26]. Consistent with this, we found that RCC-Luc cells have a 10-fold increase in *vegf-a* expression vs. the other tumor cell lines (Figure 5), which explains its robust angiogenic properties. However, the significance of these findings is limited by the toxicity and modest efficacy of drugs that specifically target VEGF-A and VEGFR-2 [27]. Thus, our primary objective for developing this xenograft model is to elucidate the factors that regulate RCC vasculogenesis, which are unknown, and may serve as superior drug targets since vasculogenesis does not occur in healthy adult tissues.

Just as gene knockout studies have demonstrated that VEGF-A is essential for the formation of the initial vascular plexus during embryogenesis [28], similar experiments have demonstrated that angiopoietins are essential for subsequent remodeling, maturation and stabilization of these vessels into vascular networks [29–31]. Transgenic mice over-expressing VEGF or Ang1 in the skin, under control of the keratin (K)-14 promoter, show increased vessel area with dissimilar morphologies [32]. Dermal vessels of K14-VEGF mice have increased length, whereas those of K14-Ang1 mice have increased diameter [33]. Additionally, dermal vessels in K14-VEGF mice are leaky (hyper-permeable) and show increased leukocyte adhesion, a cardinal sign of inflammation [32]. Interestingly, dermal vessels in K14-Ang1 mice are non-leaky [34]. Moreover, over-expression of Ang1 makes dermal vessels resistant to the increase in permeability caused by inflammatory agents or by over-expression of VEGF [34]. Based on these genetic studies a central paradigm has emerged to explain large vessel formation, such as that which occurs in RCC metastasis to bone, which posits that the initial blood vessels that form in the tumor are induced by VEGF

family members secondary to hypoxia. Subsequently, Ang factors are then responsible for the remodeling of these small leaky vessels into large vessels that promote tertiary metastases. Based on this theory a new class of biologic Ang inhibitors that signal through Tie2 have been developed for solid tumor chemotherapy. A phase I trial with AMG386 was completed in 32 patients, but none with RCC [35].

Although a clear role for Ang-induced vasculogenesis has been established in normal mammalian development, its role in cancer remains a topic of great debate. Some studies suggest that Ang-1 may be pro-angiogenic [36–38], while others have demonstrated that Ang-1 inhibits angiogenesis, tumor growth and vascular permeability [18–21, 39–41]. Moreover, the differential expression pattern of Ang-1 and Ang-2, which compete for the same Tie2 receptor, is known to be a biomarker of tumor progression, such that aggressive disease commences when Ang-2 levels exceed that of Ang-1 [18, 42, 43]. Thus, our finding that Ang1 is significantly down-regulated in RCC-Luc cells (Figure 5) is consistent with the later view, and warrants further investigation into the role of Ang1 in RCC vasculogenesis.

Another important question of RCC bone metastasis is the relative contribution of its proliferative and osteolytic potential towards its unique vascular phenotype. Several authors have noted that the osteolytic nature of RCC may, in part, be due to the interaction of the tumor with its surrounding bone environment [44, 45]. Here we demonstrate that the osteolytic and proliferative nature of the tumor cell lines studied are independent of tumor vascularity, as RCC-Luc has both modest luciferase expression (Fig. 1) and osteolytic (Fig. 2) capacity compared to the other tumor lines. Although our studies are limited by the fact that we only used one cell line for each cancer type, and that there could be other RCC in which these behaviors are dependent on each other, here we establish a model that faithfully displays the unique vascularity of RCC that is frequently seen in the clinical setting (Figs. 3 & 4). Furthermore, we proposed that this model can be used to elucidate the factors that regulate RCC-mediated vasculogenesis in bone, and assess novel therapies that interfere with this devastating part of its metastasis to bone.

Acknowledgments

The authors would like to thank Ryan Tierney and Michael Thullen for technical assistance with the histology and micro-CT analyses respectively. This work was supported by research grants from the Orthopaedic Research and Education Foundation, and the National Institutes of Health PHS awards AR54041, and University of Rochester Clinical and Translational Science Institute KL2 RR024136.

References

1. National Cancer, I. NCI Surveillance, Epidemiology and End Results (SEER) Program for statistics on Cancer. 2009.
2. Schoffski P, et al. Emerging role of tyrosine kinase inhibitors in the treatment of advanced renal cell cancer: a review. Ann Oncol. 2006; 17(8):1185–1196. [PubMed: 16418310]
3. Ng CS, et al. Renal cell carcinoma: diagnosis, staging, and surveillance. AJR.American journal of roentgenology. 2008; 191(4):1220–1232. [PubMed: 18806169]
4. Zagoria RJ, Bechtold RE. The role of imaging in staging renal adenocarcinoma. Seminars in ultrasound, CT, and MR. 1997; 18(2):91–99.
5. Kim WY, Kaelin WG. Role of VHL gene mutation in human cancer. Journal of clinical oncology : official journal of the American Society of Clinical Oncology. 2004; 22(24):4991–5004. [PubMed: 15611513]
6. Patel PH, et al. Targeting von Hippel-Lindau pathway in renal cell carcinoma. Clinical cancer research : an official journal of the American Association for Cancer Research. 2006; 12(24):7215–7220. [PubMed: 17189392]

7. Mellado B, Gascon P. Molecular biology of renal cell carcinoma. Clinical & translational oncology : official publication of the Federation of Spanish Oncology Societies and of the National Cancer Institute of Mexico. 2006; 8(10):706–710.
8. Nemeth JA, et al. Severe combined immunodeficient-hu model of human prostate cancer metastasis to human bone. Cancer Res. 1999; 59(8):1987–1993. [PubMed: 10213511]
9. McLemore TL, et al. Comparison of intrapulmonary, percutaneous intrathoracic, and subcutaneous models for the propagation of human pulmonary and nonpulmonary cancer cell lines in athymic nude mice. Cancer Res. 1988; 48(10):2880–2886. [PubMed: 3359444]
10. Yoneda T, et al. Inhibition of osteolytic bone metastasis of breast cancer by combined treatment with the bisphosphonate ibandronate and tissue inhibitor of the matrix metalloproteinase-2. J Clin Invest. 1997; 99(10):2509–2517. [PubMed: 9153295]
11. Nakai M, et al. A synthetic antagonist to laminin inhibits the formation of osteolytic metastases by human melanoma cells in nude mice. Cancer Res. 1992; 52(19):5395–5399. [PubMed: 1394144]
12. Feeley BT, et al. Overexpression of noggin inhibits BMP-mediated growth of osteolytic prostate cancer lesions. Bone. 2006; 38(2):154–166. [PubMed: 16126463]
13. He X, et al. Regulation of receptor for activated C kinase 1 protein by the von Hippel-Lindau tumor suppressor in IGF-I-induced renal carcinoma cell invasiveness. Oncogene. 2011; 30(5):535–547. [PubMed: 20871634]
14. Shi YE, et al. Antitumor activity of the novel human breast cancer growth inhibitor, mammary-derived growth inhibitor-related gene, MRG. Cancer Res. 1997; 57(15):3084–3091. [PubMed: 9242429]
15. Ionescu AM, et al. CREB Cooperates with BMP-stimulated Smad signaling to enhance transcription of the Smad6 promoter. J Cell Physiol. 2004; 198(3):428–440. [PubMed: 14755548]
16. Zhang X, et al. Periosteal progenitor cell fate in segmental cortical bone graft transplantations: implications for functional tissue engineering. Journal of bone and mineral research : the official journal of the American Society for Bone and Mineral Research. 2005; 20(12):2124–2137. [PubMed: 16294266]
17. Na X, et al. Overproduction of vascular endothelial growth factor related to von Hippel-Lindau tumor suppressor gene mutations and hypoxia-inducible factor-1 alpha expression in renal cell carcinomas. J Urol. 2003; 170(2 Pt 1):588–592. [PubMed: 12853836]
18. Ahmad SA, et al. The effects of angiopoietin-1 and -2 on tumor growth and angiogenesis in human colon cancer. Cancer Res. 2001; 61(4):1255–1259. [PubMed: 11245414]
19. Stoeltzing O, et al. Angiopoietin-1 inhibits tumour growth and ascites formation in a murine model of peritoneal carcinomatosis. Br J Cancer. 2002; 87(10):1182–1187. [PubMed: 12402160]
20. Stoeltzing O, et al. Angiopoietin-1 inhibits vascular permeability, angiogenesis, and growth of hepatic colon cancer tumors. Cancer Res. 2003; 63(12):3370–3377. [PubMed: 12810673]
21. Tian S, et al. Stabilization of breast cancer xenograft tumour neovasculature by angiopoietin-1. Br J Cancer. 2002; 86(4):645–651. [PubMed: 11870550]
22. Lin PP, et al. Patient survival after surgery for osseous metastases from renal cell carcinoma. The Journal of bone and joint surgery.American volume. 2007; 89(8):1794–1801. [PubMed: 17671020]
23. Yossepowitch O, et al. The natural history of noncastrate metastatic prostate cancer after radical prostatectomy. European urology. 2007; 51(4):940–947. discussion 947-8. [PubMed: 17125912]
24. Oya M. Renal cell carcinoma: biological features and rationale for molecular-targeted therapy. Keio J Med. 2009; 58(1):1–11. [PubMed: 19398878]
25. Kamura T, et al. Rbx1, a component of the VHL tumor suppressor complex and SCF ubiquitin ligase. Science (New York, N.Y.). 1999; 284(5414):657–661.
26. Kamura T, et al. Activation of HIF1alpha ubiquitination by a reconstituted von Hippel-Lindau (VHL) tumor suppressor complex. Proceedings of the National Academy of Sciences of the United States of America. 2000; 97(19):10430–10435. [PubMed: 10973499]
27. Ravaud A. Treatment-associated adverse event management in the advanced renal cell carcinoma patient treated with targeted therapies. Oncologist. 2011; 16 Suppl 2:32–44. [PubMed: 21346038]

28. Haigh JJ, et al. Conditional inactivation of VEGF-A in areas of collagen2a1 expression results in embryonic lethality in the heterozygous state. Development (Cambridge, England). 2000; 127(7): 1445–1453.
29. Thurston G. Complementary actions of VEGF and angiopoietin-1 on blood vessel growth and leakage. Journal of anatomy. 2002; 200(6):575–580. [PubMed: 12162725]
30. Abbott BD, Buckalew AR. Placental defects in ARNT-knockout conceptus correlate with localized decreases in VEGF-R2, Ang-1, and Tie-2. Developmental dynamics : an official publication of the American Association of Anatomists. 2000; 219(4):526–538. [PubMed: 11084652]
31. Jain RK, Mun LL. Leaky vessels? Call Ang1! Nat Med. 2000; 6(2):131–132.
32. Detmar M, et al. Increased microvascular density and enhanced leukocyte rolling and adhesion in the skin of VEGF transgenic mice. The Journal of investigative dermatology. 1998; 111(1):1–6. [PubMed: 9665379]
33. Suri C, et al. Increased vascularization in mice overexpressing angiopoietin-1. Science (New York, N.Y.). 1998; 282(5388):468–471.
34. Thurston G, et al. Leakage-resistant blood vessels in mice transgenically overexpressing angiopoietin-1. Science (New York, N.Y.). 1999; 286(5449):2511–2514.
35. Herbst RS, et al. Safety, pharmacokinetics, and antitumor activity of AMG 386, a selective angiopoietin inhibitor, in adult patients with advanced solid tumors. Journal of clinical oncology : official journal of the American Society of Clinical Oncology. 2009; 27(21):3557–3565. [PubMed: 19546406]
36. Suri C, et al. Increased vascularization in mice overexpressing angiopoietin-1. Science. 1998; 282(5388):468–471. [PubMed: 9774272]
37. Hansbury MJ, et al. Production and characterization of a Tie2 agonist monoclonal antibody. Angiogenesis. 2001; 4(1):29–36. [PubMed: 11824375]
38. Shim WS, et al. Inhibition of angiopoietin-1 expression in tumor cells by an antisense RNA approach inhibited xenograft tumor growth in immunodeficient mice. Int J Cancer. 2001; 94(1):6–15. [PubMed: 11668472]
39. Chae JK, et al. Coadministration of angiopoietin-1 and vascular endothelial growth factor enhances collateral vascularization. Arterioscler Thromb Vasc Biol. 2000; 20(12):2573–2578. [PubMed: 11116055]
40. Thurston G, et al. Angiopoietin-1 protects the adult vasculature against plasma leakage. Nat Med. 2000; 6(4):460–463. [PubMed: 10742156]
41. Hayes AJ, et al. Expression and function of angiopoietin-1 in breast cancer. Br J Cancer. 2000; 83(9):1154–1160. [PubMed: 11027428]
42. Ahmad SA, et al. Differential expression of angiopoietin-1 and angiopoietin-2 in colon carcinoma. A possible mechanism for the initiation of angiogenesis. Cancer. 2001; 92(5):1138–1143. [PubMed: 11571726]
43. Udani V, et al. Differential expression of angiopoietin-1 and angiopoietin-2 may enhance recruitment of bone-marrow-derived endothelial precursor cells into brain tumors. Neurol Res. 2005; 27(8):801–806. [PubMed: 16354539]
44. Virk MS, Lieberman JR. Tumor metastasis to bone. Arthritis Res Ther. 2007; 9 Suppl 1:S5. [PubMed: 17634144]
45. Kominsky SL, et al. MMP-13 is over-expressed in renal cell carcinoma bone metastasis and is induced by TGF-beta1. Clin Exp Metastasis. 2008; 25(8):865–870. [PubMed: 18709334]

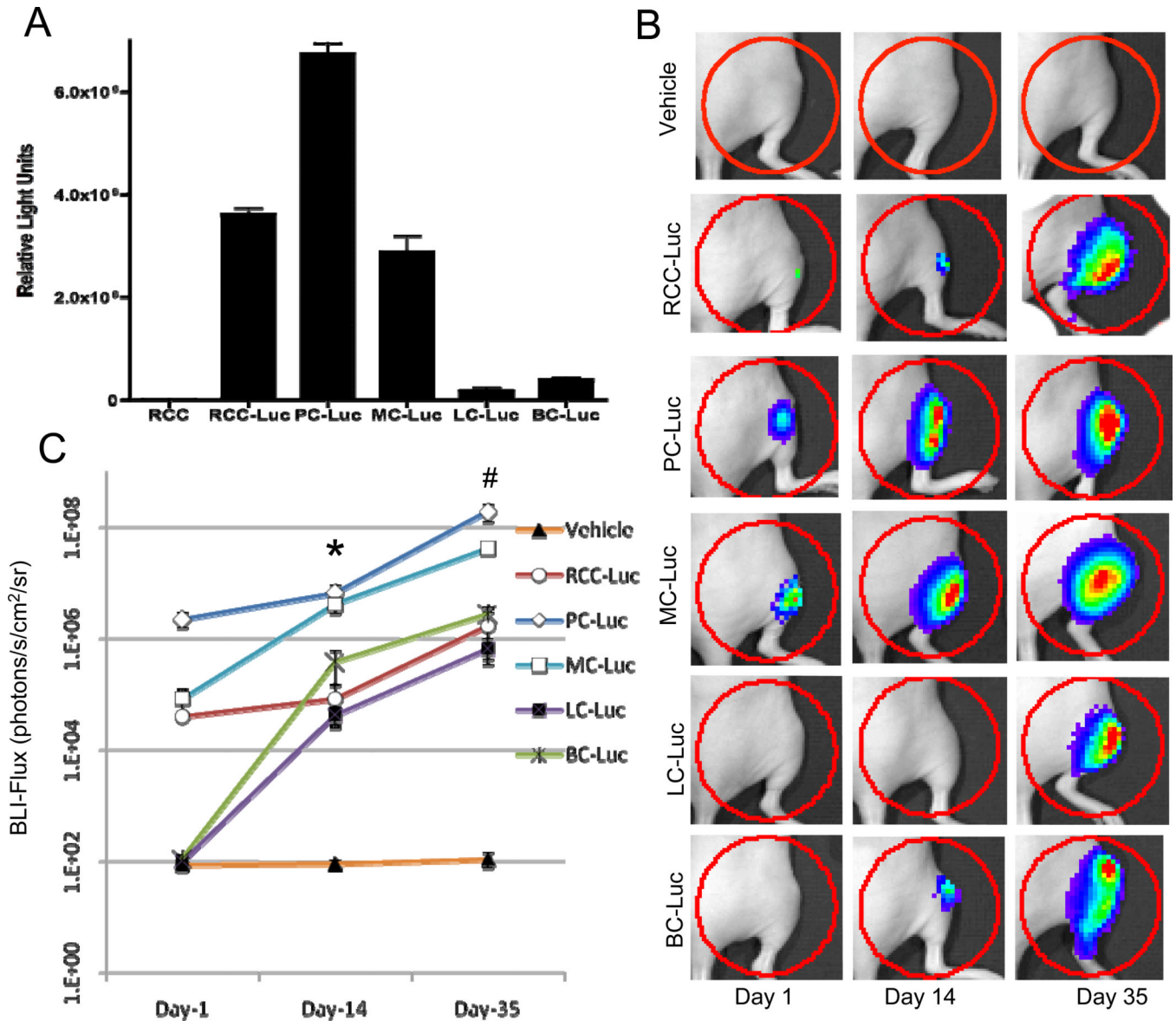

Figure 1. RCC-Luc displays moderate luciferase activity *in vitro* and *in vivo* vs. PC-Luc, MC-Luc, LC-Luc and BC-Luc

Tumor cell lines stably transfected with luciferase, and the untransfected 786-O negative control, were grown in culture and the bioluminescent signal from cells growing in log phase was determined from cell extracts *in vitro* (A). The data are presented as the mean RLU values (n=4) +/− SD. Longitudinal *in vivo* BLI was performed on athymic nude mice (n=10) following intra-tibial injection of 1×10^5 Luc transfected tumor cells, or saline (Vehicle) on days 1, 14 and 35 after injection. Representative images with a heat map of the bioluminescent signal, and the region of interest (ROI) analyzed (red circled region), are presented to illustrate the relative differences between the tumor cell lines versus the vehicle control over time (B). The BLI signal for each group is presented as the mean +/− SD at the indicated time point (C). ($p<0.05$ PC-Luc vs. RCC-Luc at day 14* and day 35#)

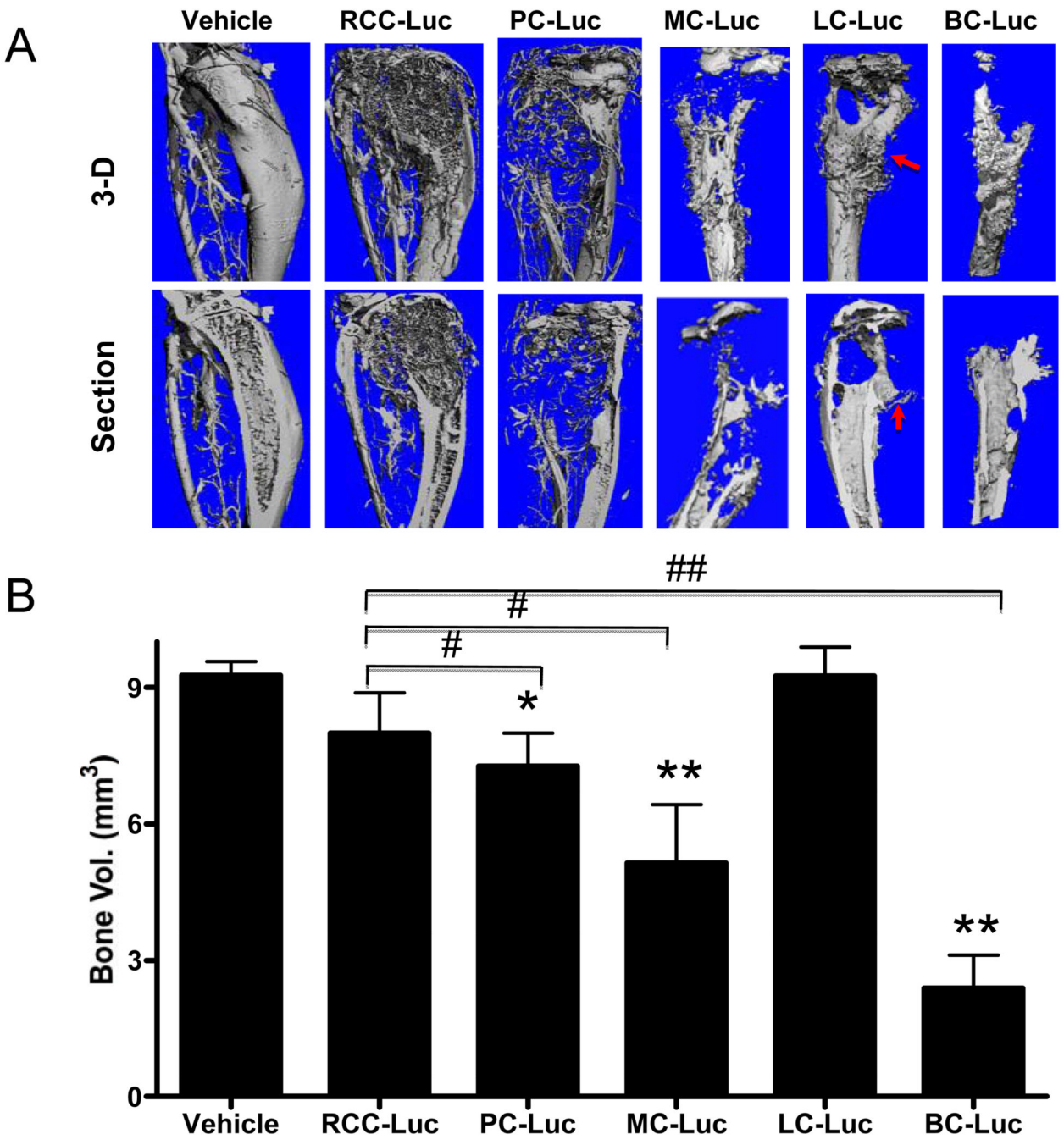

Figure 2. RCC-Luc displays modest osteolysis vs. PC-Luc, MC-Luc, LC-Luc and BC-Luc

The mice described in Figure 1 were euthanized on day 35 after intra-tibial injection during vascular perfusion with Microfil. The tumor engrafted tibiae were harvested and analyzed by micro-CT. 3D reconstructed images of a representative tibia from each group are shown from the surface (top) and medial cross-section (bottom) views (A). Note new bone formation in LC-Luc xenograft (arrow). The bone volumes were calculated for all specimens and the data are presented as the mean +/− SD for each group (* $p<0.05$,** $p<0.001$ vs. Vehicle; $^{\#}p<0.05$, $^{\#\#}p<0.001$ vs. RCC-Luc) (B).

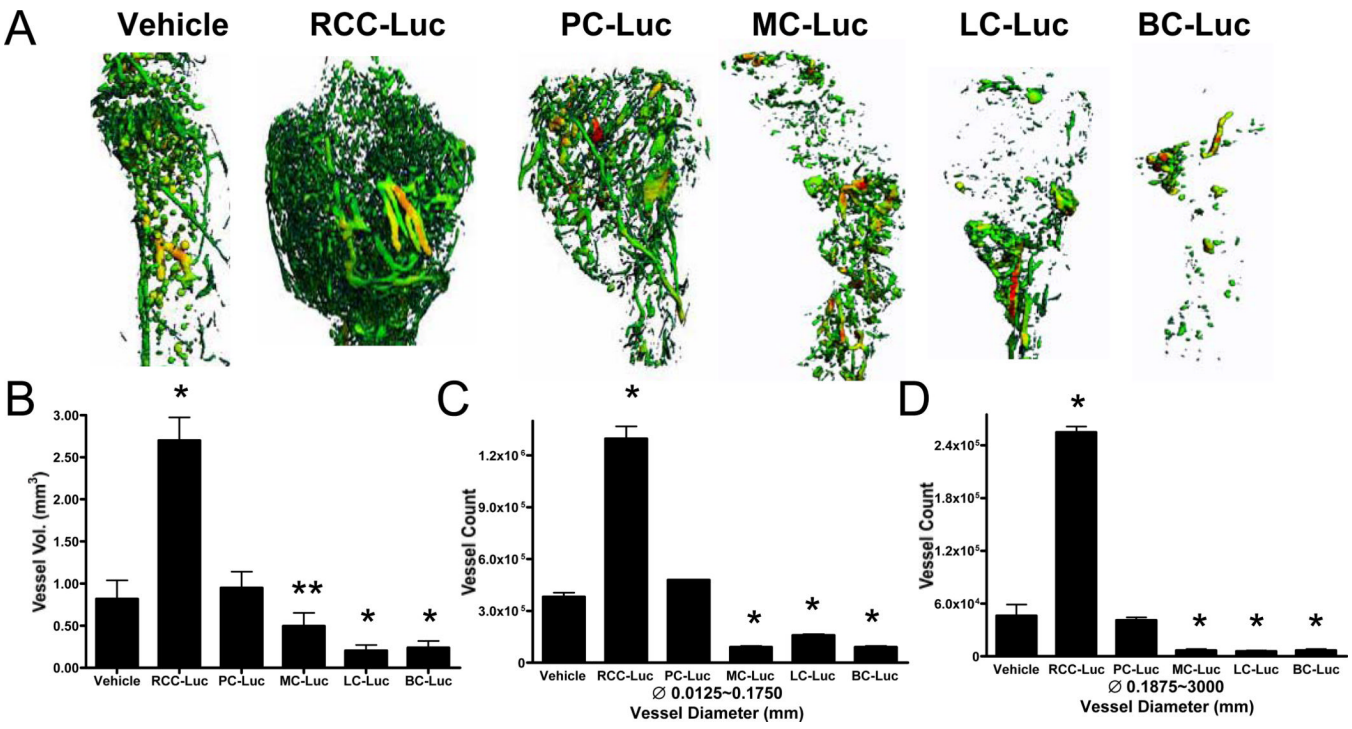

Figure 3. RCC-Luc is significantly more vascular vs. PC-Luc, MC-Luc, LC-Luc and BC-Luc

The tumor engrafted tibiae described in Figure 2 were demineralized in EDTA and reanalyzed by micro-CT to quantify the Microfil in the sample. 3D reconstructed images of the Microfil perfused vasculature are presented from representative samples from each group (A). Spectrum color is used to denote vessel size with medium and large diameter vessels shown in yellow and red (respectively). Note the remarkably larger vasculature in the RCC-Luc compared to the other samples. Computerized morphometry was performed on these samples to quantify the total vessel volume (B), and the number of small diameter (C) and large diameter (D) vessels, and the data are presented as the mean +/− SD for each group (* $p<0.001$. ** $p<0.01$ vs. Vehicle).

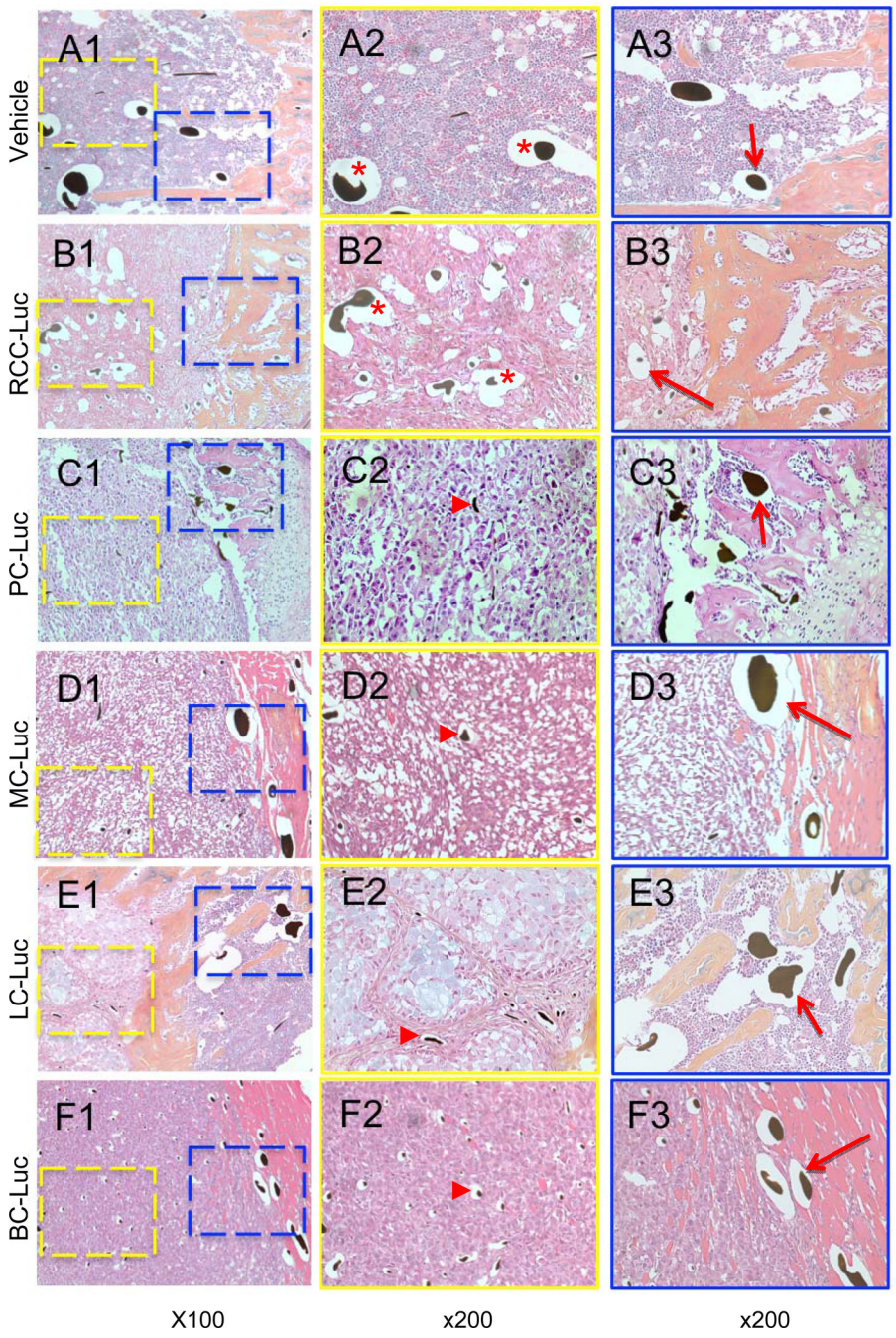

Figure 4. Tumor induced vasculogenesis is unique to RCC-Luc solid tumors in bone

The demineralized tibiae described in Figure 3 were processed for paraffin embedded histology and tissue sections were stained with hematoxylin and eosin. Representative photographs taken at 100X (A1–F1) and 200X for the tumor stroma (A2–F2, yellow box at 100 X magnified to 200 X) and surrounding parenchyma (A3–F3, blue box at 100 power magnified to 200 X) are shown respectively. Note that only RCC-Luc xenografts contain large Microfil containing vessels within the solid tumor, which were similar in size to the large vessels in normal bone marrow (red * in A2 & B2). The presence of these large Microfil containing vessels in the other xenografts was restricted to the parenchymal tissue and was similar to that observed in vehicle and RCC-Luc (red arrows in A3–F3), while only

small Microfil containing capillaries were observed in PC-Luc, MC-Luc, LC-Luc and BC-Luc tumors (red arrowheads in C2–F2).

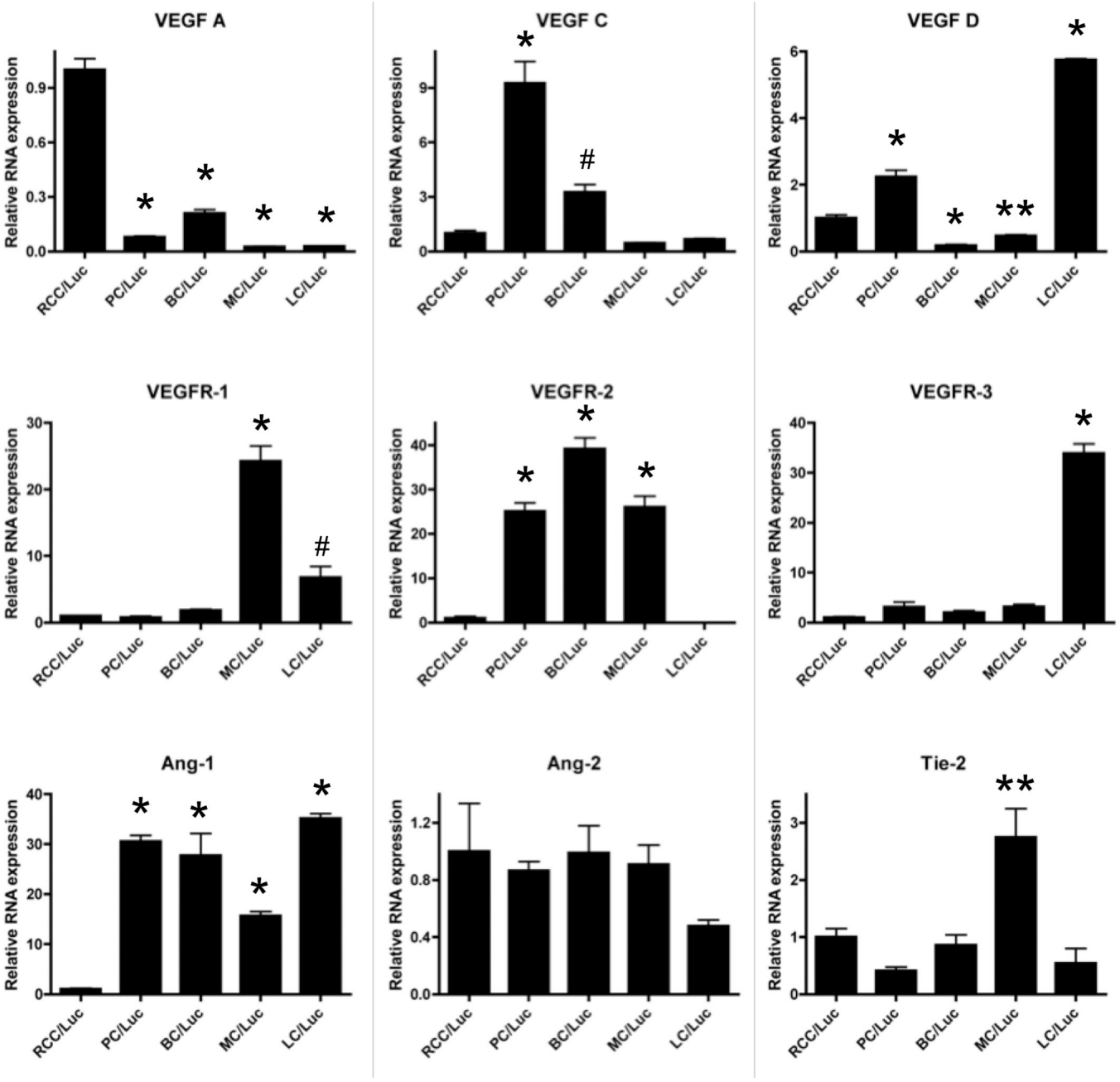

Figure 5. Vasculogenic gene expression in RCC-Luc

Quantitative reverse transcriptase PCR (qPCR) was performed to assess angiogenic/vasculogenic gene expression on all tumor cell lines. The gene expression levels were standardized to GAPDH and are presented as the fold difference from RCC-Luc (mean +/− SD; n=3; **p*<0.001, ***p*<0.01, #*p*<0.05 vs. RCC-Luc).